Pushing the Nyquist-Shannon limit: exploiting multi-fidelity observations to provide high-resolution weather maps for climate services, early warning centres and weather forecasts

Daniëlle van Beekvelt[1,2¤], Irene Garcia-Marti[2¤], Jouke de Baar[2¤],

1 Dept. of Mathematics, Utrecht University, Utrecht, Utrecht, the Netherlands

2 Dept. of Observations and Data Technology (RDWD), Royal Netherlands Meteorological Institute (KNMI), De Bilt, Utrecht, the Netherlands

¤Current Address: KNMI, Utrechtseweg 297, 3731 GA De Bilt, Utrecht, the Netherlands

* garciamarti@knmi.nl

Abstract

The pursue of a higher-resolution gridded climate data and weather forecast requires an unprecedented number of surface observations to model the sub-mesoscale. National meteorological services (NMS) have practical and financial limitations to the number of observations it can collect, therefore, opening the door to crowdsourced weather initiatives might be an interesting option to mitigate data scarcity. In recent years, scientists have made remarkable efforts at assessing the quality of crowdsourced collections and determining ways these can add value to the "daily business" of NMS. In this work, we develop and apply a multi-fidelity spatial regression method capable of combining official observations with crowdsourced observations, which enables the creation of high-resolution interpolations of weather variables. The availability of a sheer volume of crowdsourced observations also poses questions on what is the maximum weather complexity that can be modelled with these novel data sources. We include a structured theoretical analysis simulating increasingly complex weather patterns that uses the Shannon-Nyquist limit as a benchmark. Results show that the combination of

official and crowdsourced weather observations pushes further the Shannon-Nyquist limit, thus indicating that crowdsourced data contributes at monitoring sub-mesoscale weather processes (e.g. urban scales). We think that this effort illustrates well the potential of crowdsourced data, not only to expand the current range of products and services at NMS, but also opening the door for high-resolution weather forecast and monitoring, issuing local early warnings and advancing towards impact-based analyses.

Author summary

The Royal Netherlands Meteorological Institute (KNMI) is currently using data from their own weather stations that meet international standards. However, there are a lot more measurements available from for example crowd sourced weather observations that do not adhere to these standards. I want to be able to use all of this available data, because that would increase the accuracy of weather predictions. I expect the crowd sourced data to contain larger measurement inaccuracies than the KNMI measurements and therefore in order to use all of this data combined I looked in to a method that would allow me to work with high fidelity data. To test the robustness of this method I have simulated weather data for various spatial complexities, this allows me to test how the model performs for different weather phenomena. From this simulated date I have taken (noisy) samples and entered these in the model as input. By doing this I can compare the results of the model to the synthetic data and compute the errors in the computations. These tests have proven that using these multiple data sources leads to a nation-wide decrease in uncertainty for the predictions.

1 Introduction

In the past three decades, the need for high-quality gridded climate data sets has fuelled a continues increase of spatial resolution [1]. Where such data sets were initially typically provided at a ≈ 50 km resolution, current data sets are often provided at ≈ 10 km resolution [2]. However, users of such data sets ask for even higher spatial resolution, and we are currently pushing into the ≈ 1 km resolution [3].

Monitoring the recent history and present state of the local weather is an important

aspect of the work of NWS weather rooms and early warning centres. For example, monitoring temperature and precipitation at a high spatial resolution is an important part of warning for possible adverse road traffic conditions.

At the same time, weather forecasts have steadily been improving since the onset of the 1980s [4]. The inclusion of surface and satellite observations and the improvement of data assimilation methods, powered with better computational capabilities, yielded a substantial global increase in the forecast skill [4, 5]. Weather models assimilate a sheer volume of observations, thus enabling forecasts typically at the mesoscale or synoptic scales, which are adequate resolutions to monitor large phenomena. Nevertheless, modelling sub-mesoscale processes (e.g. urban or neighborhood scales) would require an unprecedented number of surface observations that National Meteorological Services (NMS) might be unable to provide.

Parallel to the improvement of the weather models has been the advent of new technological and scientific advances that have changed the way surface observations are acquired. The appearance, consolidation, and current ubiquity of wireless networks, coupled with decreasing hardware prices, implies that today the acquisition of surface observations is possible practically anywhere on Earth [6]. These favorable conditions prompted the organic (or commercial) creation of new observational networks in which participants install personal weather stations (PWS) in their available spaces (e.g. home, schools, urban parks) and start measuring the weather collaboratively.

The Royal Netherlands Meteorological Institute (KNMI) has been an active participant of such crowdsourced initiatives. In 2015, the KNMI became a partner of the Weather Observations Website (WOW) initiative, a global monitoring project conceived to provide a cloud-based platform where users can share their weather observations [7]. Currently, more than 30,000 users worldwide contribute to the WOW platform, yielding more than one million observations per day [8]. Focusing on the Dutch WOW (hereinafter: WOW-NL, http://wow.knmi.nl), the figures remain remarkable: around 1,000 stations monitor the weather in the Netherlands, yielding more than 250 million observations in nine years.

The availability of crowdsourced data collections (e.g. WOW, Netatmo) has motivated a buzzing activity around this topic across European NMS researchers in recent years. Substantial efforts have been dedicated to determine the quality of the

weather measurements [9–11], and some of these quality assurance procedures have turned into software packages used in research [12, 13]. Some of these research lines investigate the potential that crowdsourced weather data has to study small-scale weather patterns, such as urban wind [14] or tracking the movement of storm systems [15]. These efforts have been picked up by large international organizations, such as EUMETNET [16] or the ECMWF, which have manifested interest in continuing promoting the usage of these novel data sources.

We join this effort illustrating potential for crowdsourced weather data beyond weather forecasting. We think that these (near) real-time observations have high potential to contribute creating high-resolution interpolations or issuing local early warnings during severe weather conditions. In this work, we describe how we applied a data-driven multi-fidelity spatial regression method to create high-resolution interpolations for the Netherlands. This method is able to combine official observations from the KNMI network and WOW-NL observations. We provide a structured analysis simulating complex weather patterns that are illustrative of the substantial contribution that crowdsourced data can offer at pursuing the monitoring of the sub-mesoscale processes. In addition, we use the Shannon-Nyquist theorem [17] to assess how much the inclusion of WOW-NL data increases our theoretical skill to observe patterns with a higher spatial frequency (e.g. rainfall, wind). We hope these results will motivate NMS at including crowdsourced data to increase the resolution of the official products and services.

2 Data

2.1 Real-world data

The KNMI operates the network of automatic weather stations (AWS) measuring the weather in the Netherlands. This network is composed of land and sea stations (e.g. North Sea) that are mainly sited in rural or unpopulated areas, hence complying with the World Meteorological Organization (WMO) guidelines and recommendations. These official stations are composed by a set of professional-grade instruments which are regularly maintained and calibrated to ensure the best-possible measurements. AWS

measure a wide array of weather parameters (e.g. air temperature, precipitation, wind speed) every few seconds. These observations are sent to the KNMI for its subsequent inclusion in the fundamental weather products and services. The spatial distribution of the network is such so that it balances financial considerations with a good coverage for large-scale phenomena, but it implies that large local regions remain unobserved [18]. We refer to these high-quality observations as 'first-party data' (i.e. 1PD).

Nevertheless, the KNMI is not the only public organization capable of deploying sensor networks to measure weather conditions. It is the case of the Directorate General for Public Works and Water Management (i.e. Rijkswaterstaat), that maintains a network of weather stations parallel to the road network (i.e. GMS, 'Sliperiness Reporting System' in English), so that timely measurements can be acquired in the event that severe weather conditions compromise road safety. There are over 300 stations in this network, collecting basic weather parameters (i.e. temperature, precipitation, humidity). These instruments might not be as regularly maintained and calibrated as the official stations, but they tend to be reliable sources of weather observations. We refer to these good observations provided by other trusted organizations as 'second-party data' (i.e. 2PD).

However, the nature of 1PD and 2PD networks is spatially constrained, since monitoring stations require to be located in unpopulated places (e.g. rural areas, highways) to ensure the instruments are not disturbed by local factors (e.g. radiative effects). This implies that these networks are unable to acquire measurements in the urban environment, where most of the population live, and therefore local effects (e.g. urban heat islands) are poorly monitored. This spatial sparsity also limits the resolution at which NMS can offer products and services, which motivates the inclusion of weather data provided by alternative networks.

In 2015, the KNMI joined as partner the Weather Observations Website (WOW) project, a global initiative promoted by the UK Met Office, intended to collect weather observations measured by the general public. Weather enthusiasts can install in their private (e.g. at home) or public (e.g. schools, parks) spaces personal weather stations (PWS). PWS registered to this global project take weather measurements that are subsequently sent and stored in the WOW repository. The Dutch WOW (hereinafter: WOW-NL), currently comprises more than 1000 stations that have collected over 300

million observations in less than a decade. As seen, there is a sheer volume of high-resolution observations that, potentially, could help complementing the official products and services. We refer to these crowdsourced weather observations provided by the general public as 'third-party data' (i.e. 3PD).

Data quality of 3PD collections is often the main concern when it comes to integrating these observations into any research or operational chain at NMS [19]. In the past years, substantial efforts have been dedicated to the quality assurance of 3PD. In this sense, researchers at KNMI implemented a modification of an existing quality control (QC) for air temperature, and developed two QCs for wind speed [11] and precipitation [10], [20]. In general, results show that after a QC procedure intended to filter outliers and correct biases, 3PD collection seems to be of sufficient quality to be included in subsequent services, and this is in line with results obtained by other researchers (i.e. [12–14, 21]) working with 3PD.

In this research we focus on using temperature measurements from the 25th of January 2019 from the KNMI (1PD), Directorate General for Public Works and Water Management (Rijkswaterstaat, 2PD) and WOW-NL (3PD). After the QC from Napoly et al. ([9]) was applied there were 35 1PD stations, 319 2PD stations and 409 3PD stations yielding observations. The distributions of these stations can be found in Fig (1). The figures show that the 1PD stations are evenly distributed over the country, the 2PD stations follow the road network and the 3PD stations are located throughout the country, but tend to be clustered around urban and peri-urban environments.

This data will be used to make a temperature prediction for the entire country. To make this prediction we divide the Netherlands in a grid, as shown in Fig (1), for each grid point a temperature will be estimated.

We choose to work with temperature data, because there is a QC available for it and because a new method is being implemented it is easier to test it with a phenomenon such as temperature that is quite homogeneous in space and time. The robustness of the method will be tested on synthetic data that will be introduced in subsection 2.2.

Fig 1. Locations of stations. This figure shows the locations of the stations on the 25th of January 2019 that were used in this research. The first figure shows the locations of the 1PD, the second of the 2PD and the third of the 3PD.

2.2 Synthetic data

In Section 2.1 we provide a detailed description of the data sets used in this research. We consider that the weather measurements collected by the official KNMI network provide observations with reduced measurement errors, since the weather stations are regularly maintained and calibrated. However, measurement error might be larger for 2PD and 3PD monitoring networks (especially for the latter), which poses challenges to get a clear picture on how accurate the proposed model is. In addition, the high density of the combined networks (i.e. 123PD) suggests that, potentially, very complex weather patterns (i.e. quickly changing along the spatial dimensions) can be modelled, which would illustrate the robustness of the approach. In addition, an important limitation of real-world data is that we do not have a 'true map' reference to validate our interpolated grid.

The strategy to overcome these limitations is to use synthetic data capable of simulating complex weather fields that we subsequently model. Each station of the 123PD network is assigned a synthetic temperature value and measurement error. The model runs with these synthetic measurements and the resulting gridded maps can be compared on a per-point basis, hence enabling the assessment on how well the model performs. This schema has been repeated for several simulated weather patterns with different spatial variability (Figure 2). In this way, we also show that the approach is robust.

This synthetic data will look like a wavy lattice, it will be defined precisely in the next paragraph. We will use a parameter N that defines how long those waves are, i.e. how quickly the temperature changes when you move a certain distance. By defining the synthetic data like this it will be easy to see how the model behaves for weather conditions of different spatial variabilities.

The synthetic data is defined as follows, let ξ^s and ξ^g denote the station and grid point locations, respectively, given by their longitude and latitude, and let $\mathbf{y}^s$ and $\mathbf{y}^g$ denote the temperatures generated for the stations and the grid points, respectively, defined as

$$\begin{aligned} \mathbf{y}^s &= a(\cos(N\pi\xi_1^s + \psi) + \cos(N\pi\xi_2^s + \chi) + \epsilon \\ \mathbf{y}^g &= a(\cos(N\pi\xi_1^g + \psi) + \cos(N\pi\xi_2^g + \chi)). \end{aligned} \tag{1}$$

ψ and χ are defined as random numbers with $0 \leq \psi \leq 1$ and $0 \leq \chi \leq 1$. These random numbers will ensure that the temperature field is shifted a little bit, and thus make the pattern more realistic. This $\mathbf{y}$ results in a temperature field that follows a lattice pattern, where the size of the lattice fields depend on N, which is a parameter that determines how many oscillations per degree longitude and latitude there are. Furthermore, we multiply everything by amplitude a that was determined by looking at the amplitude of real measured temperature values. In addition, a synthetic error ϵ is added to $\mathbf{y}^s$, ϵ consists of a systematic error value (or 'bias') and random error value (or 'noise') for the second and third party stations. These factors, which are arbitrary to some extent, are in our set up determined by running the Kriging procedure that is described in Section 3 with data from the 25th of January and observing what values were predicted for the bias and noise. For the bias $-3.22°$C and $-2.46°$C were added to the second and third party stations respectively and $0.57°$C and $1.62°$C for the noise.

The resulting temperature fields $g(\xi^g)$ are shown for various N's in Fig (2). Temperature data has a low spatial variability, so it is expected to be similar to Fig (2)a.

Fig 2. Predictions made using synthetic data. Maps of the synthetic data generated by using Eq (1) for various values of N.

The goal of using synthetic data is to show that for weather patterns that show low spatial variability, the 1PD stations alone suffice to make accurate predictions, but when the weather pattern has higher spatial variability, using 2PD and 3PD data is beneficial. To use all of this data for making a prediction, we need a method that is able to predict values of new data points given a set of known data. In the next chapter a possible method will be addressed.

3 Methodology

In this paper we present and motivate an analytical framework for fusion of multi-fidelity multi-source data. Our approach is based on the idea that data is only complete when it is accompanied by a quantified indication of measurement error [22–24]. Because this measurement error is often not specified for all data sources, we propose to construct a simplified model of the measurement procedure, and learn the parameters of this measurement procedure model from the data set. We find that

Bayesian Data Assimilation [25] offers a natural way of modeling this measurement process, because a model of the measurement procedure is an intrinsic part of the Bayesian updating process – formalized in the 'likelihood'. In this way, our solution for dealing with bias and noise results in a natural way of fusing multi-fidelity multi-source data.

Kriging [26–28] is a probabilistic regression method that makes use of local weighting and the statistical properties of the known data points. Due to the use of statistical properties, the covariance and correlation between any two points is known, which makes it possible to compute an error map for the entire surface and that can allow us to quantify the accuracy of the prediction of the weather variable of interest. In a Bayesian framework, statistical properties also allow kriging to work with data containing bias and noise, because it is able to make estimations for the measurement error model coefficients by using maximum likelihood estimators when these coefficients are unknown [25, 29, 30]. As an alternative to maximum likelihood estimation, a resampling procedure like cross-validation might be used [31].

Kriging is closely related to Gaussian process (GP) regression [32]. In this context, a GP is a stochastic process that consists of a (possibly infinite) collection of random variables, such that every finite collection of those random variables follows a multivariate Gaussian distribution, which can be conditioned on the observed data [33, 34].

The goal of the method that uses a GP, or equivalently kriging in a Bayesian framework, is to find the distribution of the collection of random variables by learning from training data D and predicting the data Y by modelling the distribution $P(Y|D)$ as a multivariate Gaussian distribution. The process is visualised in Fig (3). In the next step a number of the samples drawn from the prior distribution are shown. After this the observations are taken in to account, the samples that are not in line with the observations are removed and a posterior distribution is computed as shown in Fig (3).

Fig 3. Visualisation of a Gaussian Process In Fig (3)a a large number of samples drawn from the prior distribution are shown, after observations are made the samples that do not reflect the observations are removed and we are left with the samples shown in Fig (3)b. The result can be summarised by a mean function.

In Bayesian kriging, we define a 'prior', which is a description of the process under

consideration before including the data. Then, we define a 'likelihood', which is a description (or approximate model) of the measurement procedure. Now, in the updating step, we introduce the observed data, which results in a 'posterior' distribution for the process under consideration. In this work, we focus on the posterior mean (the 'map') and the posterior variance (the 'uncertainty map').

For this project a modified version of kriging was used, using local error estimates (Kriging LE) [35]. In this version of kriging, bias and noise are incorporated in the computations through the likelihood. However, before we discuss this modified version the standard simple kriging will be discussed.

3.1 Bayesian data assimilation without bias and noise

Kriging is a non-parametric approach for estimating an unknown spatial process $\mathbf{X}$. kriging aims to estimate a distribution over all possible functions realisations that fit the observed data. It defines the prior on $\mathbf{X}$ as a GP [25, 33, 34, 36, 37]:

$$\mathbf{X} \sim \mathcal{N}(\mu, \mathbf{P}) \tag{2}$$

with mean μ and process covariance matrix $\mathbf{P}$. For some fields of research this might be an unconventional notation, but keep in mind that $\mathbf{X}$ represents the (so far unknown) value of the variable of interest evaluated at the grid locations and $\mathbf{P}$ represents the (so far also unknown) spatial covariance ot the value of the variable of interest evaluated between pairs of grid locations.

We then assume the normal likelihood for the observations [25]:

$$\mathbf{y}|\mathbf{X} \sim \mathcal{N}(\mathbf{HX}, \mathbf{R} = 0) \tag{3}$$

where $\mathbf{H}$ is an observation matrix. In our case, this matrix $\mathbf{H} \in \mathbb{R}^{n \times p}$ indicates where the n measurement points are located relative to the p points for which we want to predict a value – however, $\mathbf{H}$ can also define a measurement procedure that averages the quantity of interest over an interval in time or space, or any other linear operation that is a description of the measurement procedure (e.g. a partial derivative operator [38], etc.). Note that we have written $\mathbf{R} = 0$, although for numerical reasons we implement a

regularization $\mathbf{R} = \varepsilon^2\mathbf{I}$, with ε^2 in the order of machine precision [38].

After conditioning on the observed data $\mathbf{y}$, the posterior is defined by [25]:

$$\mathbf{y}|\mathbf{Y} \sim \mathcal{N}(\mathbf{y}, C) \tag{4}$$

where the posterior mean is:

$$\mathrm{E}[\mathbf{X}|\mathbf{y}] = \mu + K(\mathbf{y} - \mathbf{H}\mu) \tag{5}$$

and the posterior covariance is:

$$C = \mathrm{cov}[\mathbf{X}|\mathbf{y}] = (\mathbf{I} - K\mathbf{H})\mathbf{P} \tag{6}$$

where we have introduced the Kalman gain:

$$K = \mathbf{P}\mathbf{H}^T(\mathbf{H}\mathbf{P}\mathbf{H}^{\mathbf{T}})^{-1} \tag{7}$$

The components of covariance matrix $\mathbf{P}$ are modeled by $\mathbf{P}_{i,j} = \kappa(\mathbf{x}_i, \mathbf{x}_j)$, where κ is a positive definite kernel. We have this requirement that κ must be positive definite, to make sure that $\mathbf{P}$ is positive (semi) definite [33]. There are several different kernels, but here we will be using the kernel defined as follows

$$\kappa = \sigma^2\psi_{i,j} \tag{8}$$

where σ^2 is the variance of $\mathbf{y}$ and $\psi_{i,j}$ is the basis function corresponding to the correlation between locations

$$\psi_{i,j} = \exp\Big(-\sum_{k=1}^{d}\frac{||h_{i,j}||^2}{2\hat{\theta}_k^2}\Big) \tag{9}$$

with d being the number of dimensions and h the spatial distance between locations. $\hat{\theta} \in \mathbb{R}^d$ is a spatial parameter that we can think of as an indicator that tells us how quickly the function changes when location j moves closer or further away from location i [39, 40].

To approximate $\hat{\theta}$, we use a maximum likelihood estimator (MLE) with respect to θ,

which is equivalent to minimising [41–43]

$$L(\theta) = \log(|\mathbf{HPH}^T|) + (\mathbf{y} - \mathbf{H}\mu)^T(\mathbf{HPH}^T)^{-1}(\mathbf{y} - \mathbf{H}\mu). \tag{10}$$

The product $\mathbf{HPH}^T \in \mathbb{R}^{n\times n}$ can be interpreted as the matrix of correlations between sample data.

3.2 Bayesian data assimilation with bias and noise

However, all observed data contains bias and noise, so a method that is able to deal with that is needed. Therefore, we introduce Kriging LE, which is a version of simple kriging that is equipped to handle this. In the Bayesian framework, the bias and noise, as an intrinsic part of the measurement procedure, can be included in a natural way in the likelihood [3, 25, 35, 38, 42, 44]:

$$\boldsymbol{y}|\boldsymbol{X} = \mathcal{N}(HX + HB\boldsymbol{\beta}_B, R = IHN^2\boldsymbol{\beta}_N^2). \tag{11}$$

In Eq (11), $B\boldsymbol{\beta}_B$ is a linear model for the bias, containing bias budget B and coefficients $\boldsymbol{\beta}_B$. For example, the bias budget can contain the type of measurement device, indicating that one type of device might lead to a different bias than another type of device. However, other indicators can also be included in the bias budget. The corresponding coefficients $\boldsymbol{\beta}_B$ are estimated by including them in the MLE.

In a similar way, in Eq (11), $Nbs\beta_N$ is a linear model for the variance of the observational noise. Again, the noise budget N can contain the type of measurement device, but can also contain other proxies for the noise level of the data. Again, the corresponding coefficients $\boldsymbol{\beta}_N$ are estimated by including them in the MLE.

It is worth mentioning that the regression result is robust against estimating the noise from an MLE. As an illustration, Fig (4) shows how, for a different number of low-fidelity points in the example of Fig (3), the relative RMS prediction error has a robust minimum for a range of estimated noise levels. In addition, we observe from this illustration that the robustness increases when we have more low-fidelity data points. In other words, for the resulting map it is not essential that we find very accurate values for $\boldsymbol{\beta}_N$.

Fig 4. The regression error under different noise levels The accuracy of the interpolation depends on the true noise level and the estimated noise level. However, as can be seen from this illustration, the regression error is robust against changes in the estimated noise level.

Providing a bias and noise budget allows us to differentiate between the various data sources. In addition, although we do not use this in the present work, it is possible to include other proxies in the bias or noise budget. For example, it is possible to include population density as a proxy for observational noise, as for example in [44]. This, in essence, is how the Bayesian likelihood, as a model of the measurement procedure, allows us to have an analytical framework for multi-fidelity multi-source data fusion.

4 Results

4.1 Results for synthetic data

Recall that we had defined synthetic data for the stations and grid points. This was done to be able to illustrate the robustness of our approach. We expect that the predictions using 1PD, 12PD and 123PD all perform well if the number of oscillations N is low, but we expect 12PD and 123PD to out perform 1PD when the number of oscillations increases. This is expected, because of the Shannon-Nyquist theorem [45].This theorem states that the more oscillations there are, the more measurement points are needed to be able to identify these oscillations. We expect that the use of 2PD and 3PD will push back the Shannon-Nyquist limit, resulting in the ability to observe weather patterns of higher spatial frequency (i.e. more oscillations). This would imply that by using 2PD and 3PD we will be able to make more accurate predictions for weather phenomena with a high spatial variability.

To verify these expectations, we computed the fitting performance based on weather complexity. The results are shown in Fig (5). For each combination of parties the model was ran 5 times, each time with a different small shift in the synthetic data. The figure confirms our expectations, for a low value of N all parties perform similarly. However, as N increases there are clear differences visible between the performances. 1PD reaches its Shannon-Nyquist limit relatively quickly, while the others are still performing reasonably well. By adding more data the Shannon-Nyquist limit is pushed back

further, which implies that using more data increases the accuracy of the predictions in instances when there is a high spatial variability.

It is also notable that while 13PD has more measurements available than 12PD, it does perform a little worse than 12PD between $N \approx 1$ and $N \approx 8$. This is due to the fact that 2PD measurements are more accurate than 3PD measurements and for low N the quality of measurements is more important than the quantity of measurements.

Fig 5. Fitting performance based on weather complexity This figure shows the RMSE values for different combinations of 1PD, 2PD and 3PD for various levels of spatial variability of the data. It shows that for low spatial variability they all perform equally well, but after approximately 1.5 oscillations per degree 1PD performs significantly worse than the others.

The findings of Fig (5) are supported by the resulting maps of the predictions. In Fig (6) the results are shown for $N = 1.5$. Fig (6)a shows what the true synthetic temperature field looked like, and the other three maps show the predictions the model made using 1PD, 12PD and 123PD respectively. In Fig (7) the uncertainty of these three predictions are shown. In Fig (6)a it seems like the predicted temperatures resemble the true temperatures quite well, but when we look at the uncertainty of this prediction in Fig (7)a it is visible that there are quite large areas where the prediction is still very uncertain, like in the north of the country. The predictions made by using 12PD and 123PD are still similar for this N, but 123PD performs slightly better as can be seen from the 'average uncertainty'. However they are both a great improvement from just 1PD and have managed to reduce the uncertainty a lot in certain areas, like in the north of the country.

Fig 6. Temperature predictions for $N = 1.5$ (6)a shows the true synthetic temperature field and the following figures the predictions made by using 1PD, 12PD and 123PD respectively.

Fig 7. Uncertainty predictions for $N = 1.5$ The figures show the uncertainty of the predictions made by using 1PD, 12PD and 123PD from Fig (6) respectively.

An example that shows the potential of using 2PD and 3PD even clearer is the case of $N = 7$. The results of the prediction are shown in Fig (8) and their uncertainty in Fig (9). It shows that for 1PD the prediction in Fig (8)b does not resemble the true synthetic weather pattern shown in Fig (8)a at all, which is also substantiated by the

uncertainty computations visualised in Fig (9)b. The prediction made by 12PD shown in Fig (8)c is already much better, the true pattern is becoming visible and the average prediction uncertainty has been reduced by roughly 2 degrees Celsius. However, the pattern still seems a bit faded and in some areas of the countries, like the north, the prediction is patchy. This is also reflected in the uncertainty map in Fig (8)c. It shows there are large areas where the prediction uncertainty is very significant. Unlike in the $N = 1.5$ case, there is now a significant improvement visible between using 12PD and 123PD. The true temperature pattern is becoming more clear in Fig (8)d and the patchiness is reduced. In Fig (9)d it can be seen that the areas with a large uncertainty are greatly reduced compared to the 12PD prediction.

Fig 8. Temperature predictions for $N = 7$ Fig (8)a shows the true synthetic temperature field and the following figures the predictions made by using 1PD, 12PD and 123PD respectively.

Fig 9. Uncertainty predictions for $N = 7$ The figures show the uncertainty of the predictions made by using 1PD, 12PD and 123PD from Fig (8) respectively.

4.2 Results for real-world data

The previous section used synthetic data to demonstrate that when weather phenomena with a high spatial variability is being modeled, it is beneficial to use 2PD and 3PD in addition to 1PD. However, we would also like to see how the model behaves with real data. Therefore the model was applied to temperature data from the 25th of January 2019. Note that temperature fields do not exhibit high spatial variability so we expect 1PD, 12PD and 123PD to all perform well and to not see large performance differences between them.

The results support these expectations, when we look at the temperature maps in Fig (10) there are not any major differences. This is also expressed in the uncertainty maps shown in Fig (11). The average uncertainty is low for all three, but we do see a small decrease in the uncertainty when going from 1PD to 12PD to 123PD.

Fig 10. Temperature predictions for real world data Temperature predictions for real temperature data from the 25th of January 2019. These figures show the predictions made by using 1PD, 12PD and 123PD respectively.

Fig 11. Uncertainty predictions for real world data Uncertainty predictions for the predictions shown in Fig (10).

5 Conclusion

The Kriging LE method has been introduced as a spatial regression method that allows us to deal with multi-fidelity data, because it is able to make estimations for spatial, bias and noise parameters. The adjustment of the parameters is necessary to make accurate predictions, since 2PD and 3PD are assumed not to be as precise as 1PD. Kriging LE has been tested for two scenarios, using synthetic data and real data. The experiment with synthetic data shows that the current approach might be useful to model weather phenomena with high spatial variability when 1PD is combined with 2PD and 3PD. The experiment with real data shows that the predicted temperature fields average standard deviations decreases when 1PD is combined with 2PD and 3PD, which tells us there is potential for significant improvement when including 2PD and 3PD. This means that second and third party data can be used to increase the spatial resolution of observation-based weather interpolations and that they can be used to ensure that the nation wide prediction uncertainty is decreased significantly, especially for phenomena such as rain and wind.

Future work might be developed along two lines: 1) assessing the network design based on the spatial distribution of the stations; 2) uncertainty decrease based on bias and noise budgets. The pursue of an optimal network design is motivated by the fact that 2PD and 3PD stations are often not evenly distributed over the country, hence forming clusters. For regions with a high station density, it would be interesting to research whether all the stations are needed or some of them are redundant. This has practical implications during the modelling phase, since a non-redundant network design might reduce the computational time. Network design can also be tackled for the regions with low station density, since it might be relevant to assess where more stations are required to decrease the prediction uncertainty. In this line of uncertainty decrease, it is important to mention that in this work we have estimated a bias and noise variable for each party (i.e. type of network). However, the bias and noise could also be estimated from "bias or noise budgets" that includes sensor types, station siting conditions, or even proxies (e.g. population density, local cooling or radiative effects).

By doing this, the bias and noise can be estimated more accurately and thus the model would perform better. A disadvantage of this approach would be that it might substantially increase the computational time.

In recent years, there has been an intense research activity around the usage and incorporation of crowdsourced data in the climate sciences. Substantial efforts have been carried out to perform quality assessment for crowdsourced data [16], fitting these novel observations into the numerical weather predictions [21, 46], or defining workflows to transform these observations into valuable new products and services for NMS [18]. In this line, the current work illustrates how crowdsourced data enable the creation of high-resolution weather products, which has a remarkable potential to expand the current products and services at KNMI. The availability of these high-resolution maps, might also be helpful at issuing local weather warning and events, particularly in urban areas, and open the door to carry out impact-based analyses.

6 Acknowledgments

We would like to thank everyone involved in the WOW-project. This research has only been possible because of all the people who have a PWS and connected it to the WOW network. Due to their effort we have been given access to a lot of useful weather data that has inspired this research. We would also like to thank Rijkswaterstaat for sharing their data with us.

References

1. Daly C, Taylor G, Gibson W, Parzybok T, Johnson G, Pasteris P. High-quality spatial climate data sets for the United States and beyond. Transactions of the ASAE. 2000;43(6):1957.

2. van den Besselaar EJM, Haylock MR, van der Schrier G, Klein Tank AMG. A European daily high-resolution observational gridded data set of sea level pressure. Journal of Geophysical Research: Atmospheres. 2011;116(D11). doi:https://doi.org/10.1029/2010JD015468.

3. de Baar J, Garcia-Marti I, van der Schrier G. Spatial regression of multi-fidelity meteorological observations using a proxy-based measurement error model. Proceedings of EMS Bonn 2022, under review. 2022;.

4. Bauer P, Thorpe A, Brunet G. The quiet revolution of numerical weather prediction. Nature. 2015;525(7567):47–55.

5. Alley RB, Emanuel KA, Zhang F. Advances in weather prediction. Science. 2019;363(6425):342–344.

6. Chiaravalloti RM, Skarlatidou A, Hoyte S, Badia MM, Haklay M, Lewis J. Extreme citizen science: Lessons learned from initiatives around the globe. Conservation Science and Practice. 2022;4(2):e577.

7. Kirk PJ, Clark MR, Creed E. Weather observations website. Weather. 2021;76(2):47–49.

8. Mylne K, Male H, Gilbert S. The Weather Observations Website. Copernicus Meetings; 2022.

9. Napoly A, Grassmann T, Meier F, Fenner D. Development and application of a statistically-based quality control for crowdsourced air temperature data. Frontiers in Earth Science. 2018;6:118.

10. De Vos L, Overeem A, Leijnse H, Uijlenhoet R. Rainfall estimation accuracy of a nationwide instantaneously sampling commercial microwave link network: Error dependency on known characteristics. Journal of atmospheric and oceanic technology. 2019;36(7):1267–1283.

11. Chen J, Saunders K, Whan K. Quality control and bias adjustment of crowdsourced wind speed observations. Quarterly Journal of the Royal Meteorological Society. 2021;147(740):3647–3664.

12. Båserud L, Lussana C, Nipen TN, Seierstad IA, Oram L, Aspelien T. TITAN automatic spatial quality control¡? xmltex\break?¿ of meteorological in-situ observations. Advances in Science and Research. 2020;17:153–163.

13. Fenner D, Bechtel B, Demuzere M, Kittner J, Meier F. CrowdQC+—a quality-control for crowdsourced air-temperature observations enabling world-wide urban climate applications. Frontiers in Environmental Science. 2021;9:553.

14. Droste AM, Heusinkveld BG, Fenner D, Steeneveld GJ. Assessing the potential and application of crowdsourced urban wind data. Quarterly Journal of the Royal Meteorological Society. 2020;146(731):2671–2688.

15. Mandement M, Caumont O. Contribution of personal weather stations to the observation¡? xmltex\break?¿ of deep-convection features near the ground. Natural Hazards and Earth System Sciences. 2020;20(1):299–322.

16. Hahn C, Garcia-Marti I, Sugier J, Emsley F, Beaulant AL, Oram L, et al. Observations from Personal Weather Stations—EUMETNET Interests and Experience. Climate. 2022;10(12):1–14. doi:10.3390/cli10120192.

17. Shannon CE. Communication in the Presence of Noise. Proceedings of the IRE. 1949;37(1):10–21. doi:10.1109/jrproc.1949.232969.

18. Garcia-Marti I, Overeem A, Noteboom JW, de Vos L, de Haij M, Whan K. From proof-of-concept to proof-of-value: Approaching third-party data to operational workflows of national meteorological services. International Journal of Climatology. 2022;.

19. Bell S, Cornford D, Bastin L. How good are citizen weather stations? Addressing a biased opinion. Weather. 2015;70(3):75–84.

20. van Andel J. Quality control development for near real-time rain gauge networks for operational rainfall monitoring; 2021.

21. Hintz KS, Vedel H, Kaas E. Collecting and processing of barometric data from smartphones for potential use in numerical weather prediction data assimilation. Meteorological Applications. 2019;26(4):733–746.

22. BIPM, ISO. Guide to the Expression of Uncertainty in Measurement. Geneva, Switzerland. 1995;122:16–17.

23. Kessel W. Measurement uncertainty according to ISO/BIPM-GUM. Thermochimica Acta. 2002;382(1-2):1–16.

24. Duvernoy J. Guidance on the computation of calibration uncertainties. World Meteorological Organization. 2015;.

25. Wikle CK, Berliner LM. A Bayesian tutorial for data assimilation. Physica D: Nonlinear Phenomena. 2007;230(1-2):1–16.

26. Matheron G. Principles of geostatistics. Economic geology. 1963;58(8):1246–1266.

27. Gandin LS. Objective analysis of meteorological fields. Israel program for scientific translations. 1963;242.

28. Cressie N. The origins of kriging. Mathematical geology. 1990;22(3):239–252.

29. Azpurua MA, Dos Ramos K. A comparison of spatial interpolation methods for estimation of average electromagnetic field magnitude. Progress In Electromagnetics Research M. 2010;14:135–145.

30. Tatalovich Z, Wilson JP, Cockburn M. A comparison of thiessen polygon, kriging, and spline models of potential UV exposure. Cartography and Geographic Information Science. 2006;33(3):217–231.

31. James G, Witten D, Hastie T, Tibshirani R. An introduction to statistical learning. vol. 112. Springer; 2013.

32. Williams CK, Rasmussen CE. Gaussian processes for machine learning. vol. 2. MIT press Cambridge, MA; 2006.

33. Quadrianto N, Kersting K, Xu Z. In: Gaussian Process. Boston, MA: Springer US; 2010. p. 428–439.

34. Murphy KP. Machine learning: a probabilistic perspective. MIT press;.

35. de Baar JH, Percin M, Dwight RP, van Oudheusden BW, Bijl H. Kriging regression of PIV data using a local error estimate. Experiments in fluids. 2014;55:1–13.

36. Weinberger K. Lecture 15: Gaussian Processes; 2018. Machine Learning for Intelligent Systems, Course page. Available from: `https://www.cs.cornell.edu/courses/cs4780/2018fa/lectures/lecturenote15.html`.

37. Shekaramiz M, Moon TK, Gunther JH. A Note on Kriging and Gaussian Processes. 2019;.

38. de Baar JH, Dwight RP, Bijl H. Improvements to gradient-enhanced Kriging using a Bayesian interpretation. International Journal for Uncertainty Quantification. 2014;4(3).

39. Tobler WR. A computer movie simulating urban growth in the Detroit region. Economic geography. 1970;46(sup1):234–240.

40. Forrester AI, Sóbester A, Keane AJ. Multi-fidelity optimization via surrogate modelling. Proceedings of the royal society a: mathematical, physical and engineering sciences. 2007;463(2088):3251–3269.

41. Mardia KV, Marshall RJ. Maximum likelihood estimation of models for residual covariance in spatial regression. Biometrika. 1984;71(1):135–146.

42. Forrester AI, Keane AJ, Bressloff NW. Design and analysis of" Noisy" computer experiments. AIAA journal. 2006;44(10):2331–2339.

43. De Baar JH, Dwight RP, Bijl H. Fast maximum likelihood estimate of the Kriging correlation range in the frequency domain. IAMG 2011: Proceedings of the International Association of Mathematical Geosciences" Mathematical Geosciences at the Crossroads of Theory and Practice", Salzburg, Austria, 5-9 September 2011. 2011;.

44. de Baar J, Garcia-Marti I. Recent improvements in spatial regression of climate data. NATO Research Workshop AVT-354 on Multi-fidelity methods for military vehicle design. 2022;.

45. Por E, van Kooten M, Sarkovic V. Nyquist–Shannon sampling theorem. Leiden University. 2019;1:1.

46. Nipen TN, Seierstad IA, Lussana C, Kristiansen J, Hov Ø. Adopting citizen observations in operational weather prediction. Bulletin of the American Meteorological Society. 2020;101(1):E43–E57.

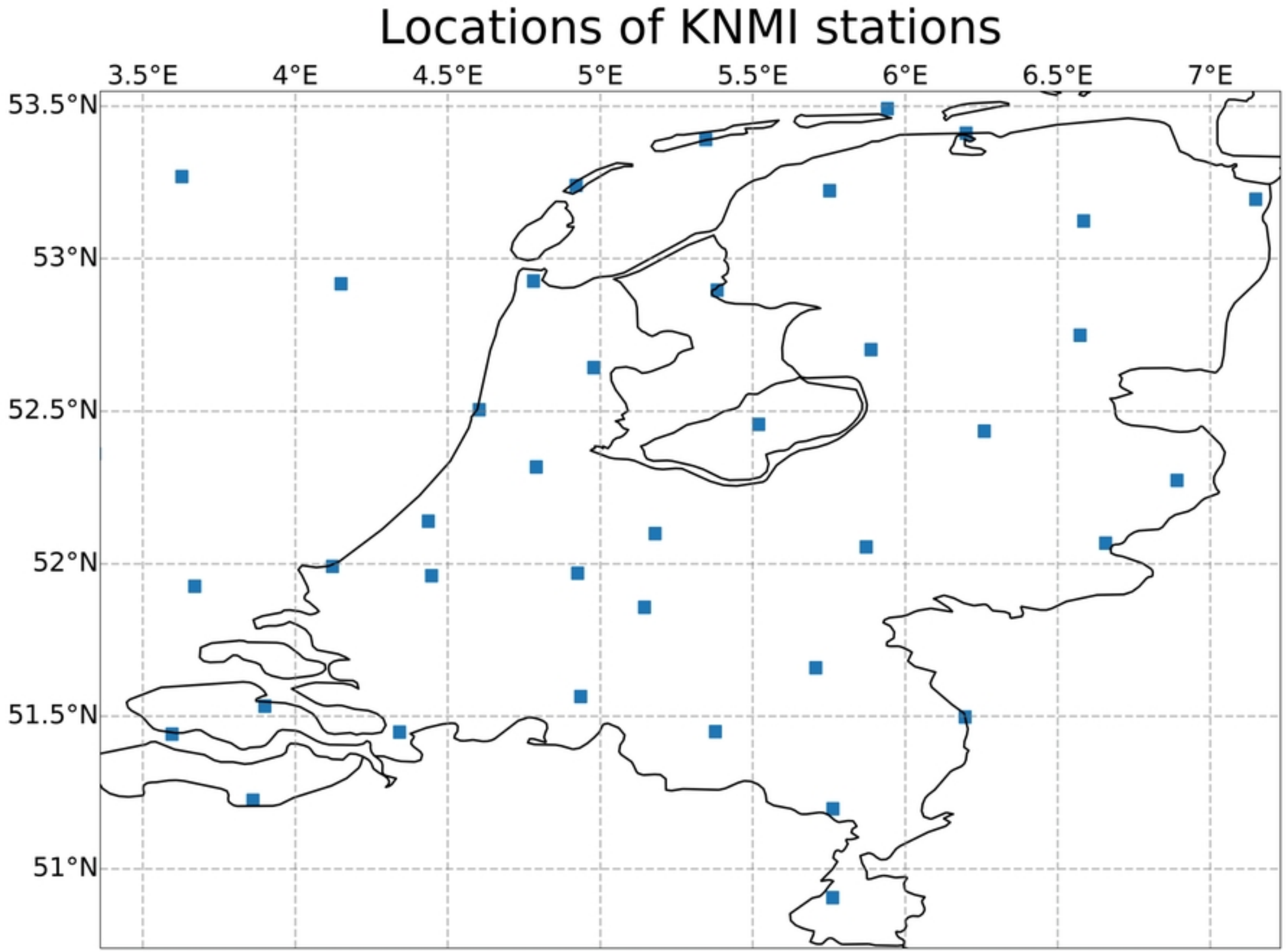
Locations of KNMI stations
3.5°E
4°E
4.5°E
5°E
5.5°E
6°E
6.5°E
7°E
53.5°N
53°N
52.5°N
52°N
51.5°N
51°N

Figure1

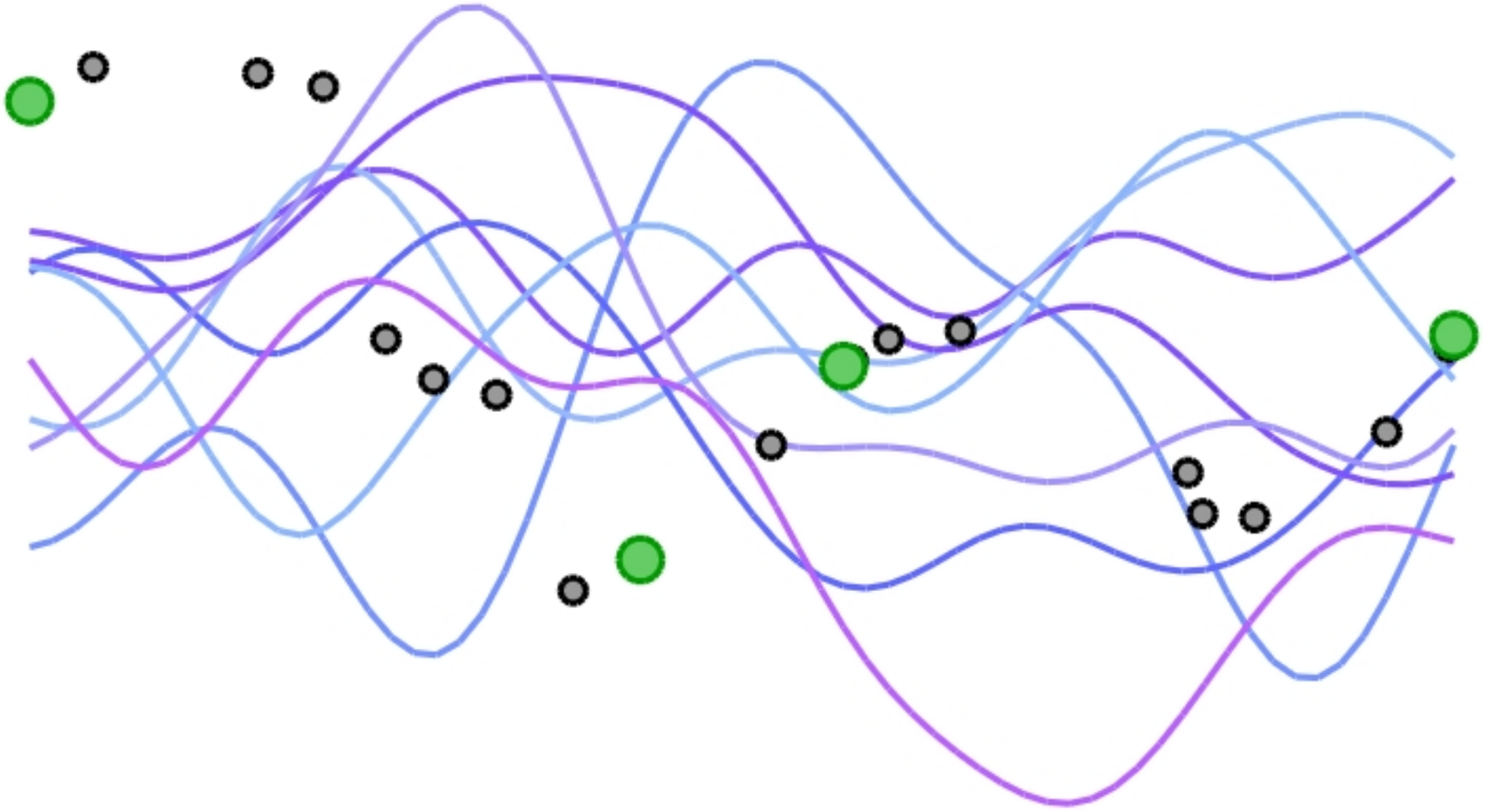

Figure3

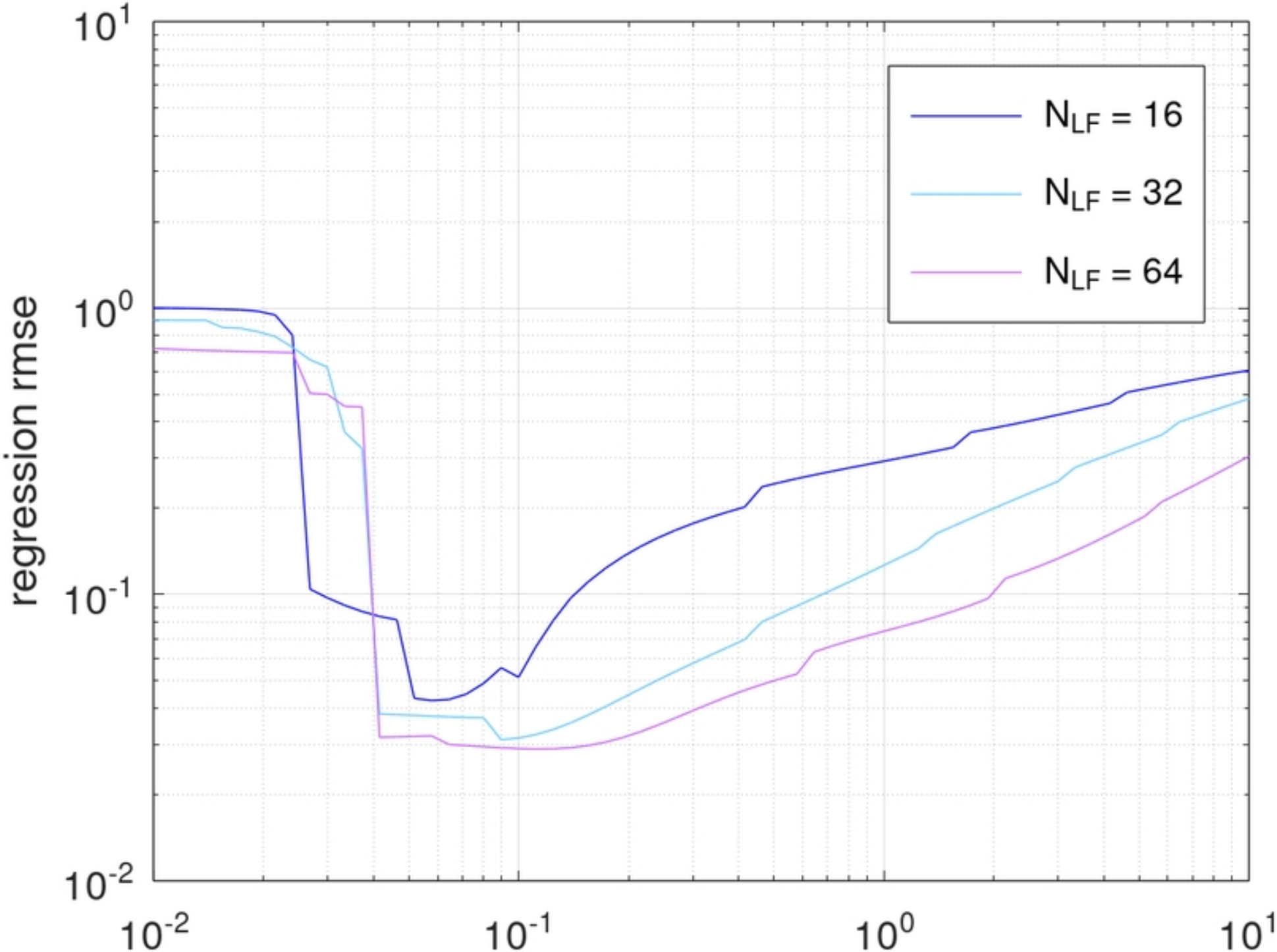
10^1
10^0
10^{-1}
10^{-2}
regression rmse
10^{-2}
10^{-1}
10^0
10^1
estimated noise level
N_{LF} = 16
N_{LF} = 32
N_{LF} = 64

Figure4

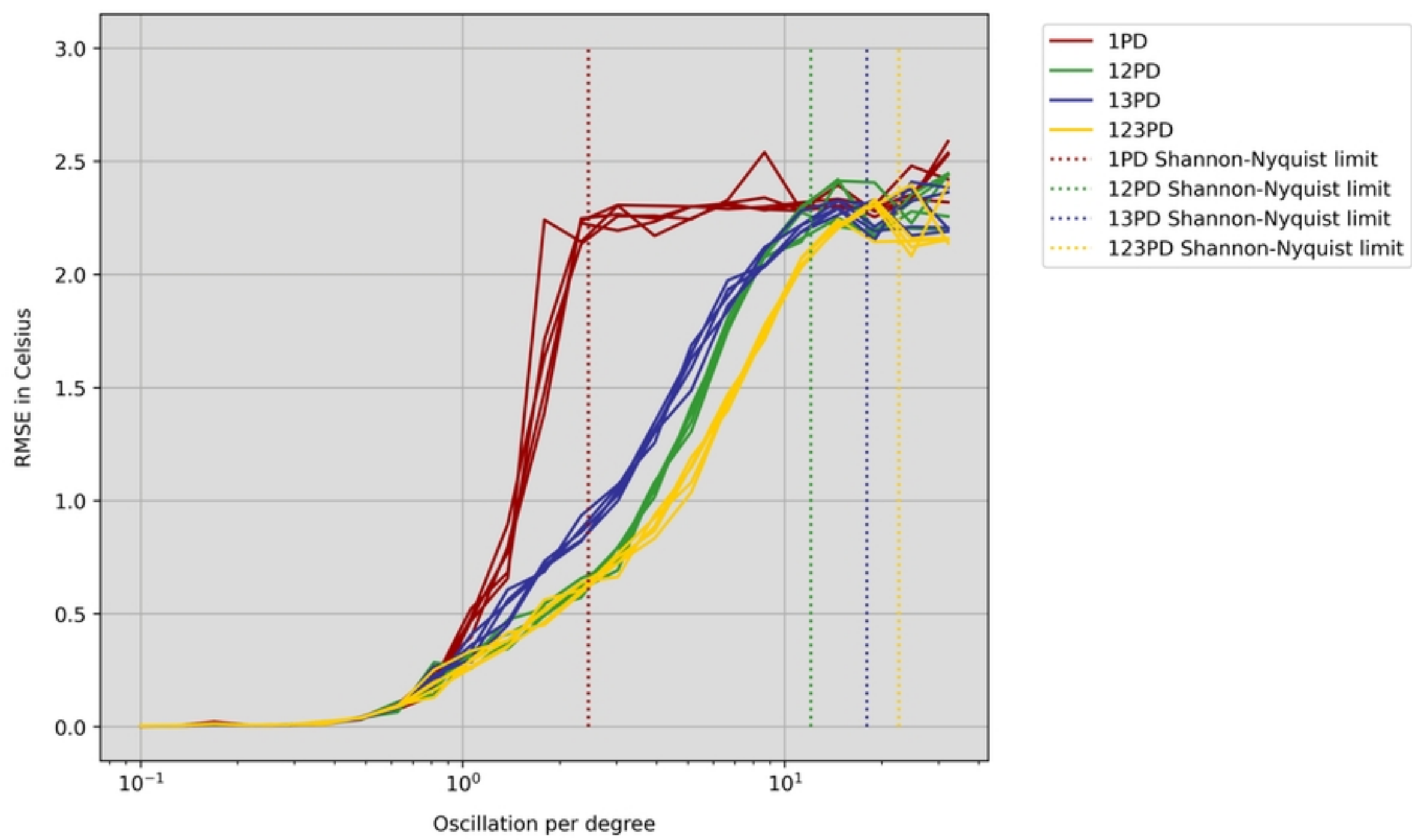
1PD
12PD
13PD
123PD
1PD Shannon-Nyquist limit
12PD Shannon-Nyquist limit
13PD Shannon-Nyquist limit
123PD Shannon-Nyquist limit
RMSE in Celsius
Oscillation per degree
3.0
2.5
2.0
1.5
1.0
0.5
0.0
10^{-1}
10^{0}
10^{1}

Figure5

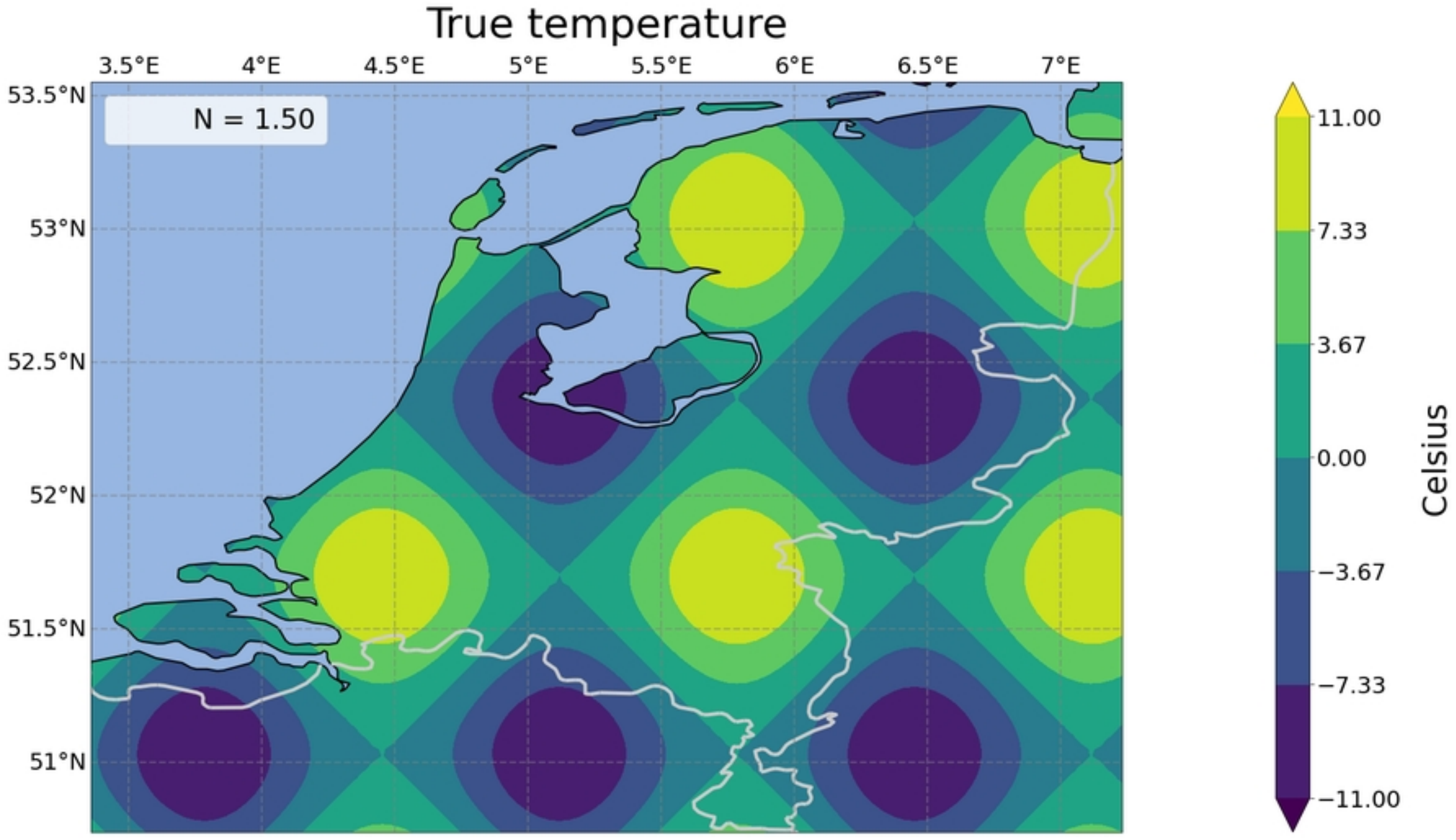
True temperature
3.5°E
4°E
4.5°E
5°E
5.5°E
6°E
6.5°E
7°E
53.5°N
53°N
52.5°N
52°N
51.5°N
51°N
N = 1.50
11.00
7.33
3.67
0.00
−3.67
−7.33
−11.00
Celsius

Figure6

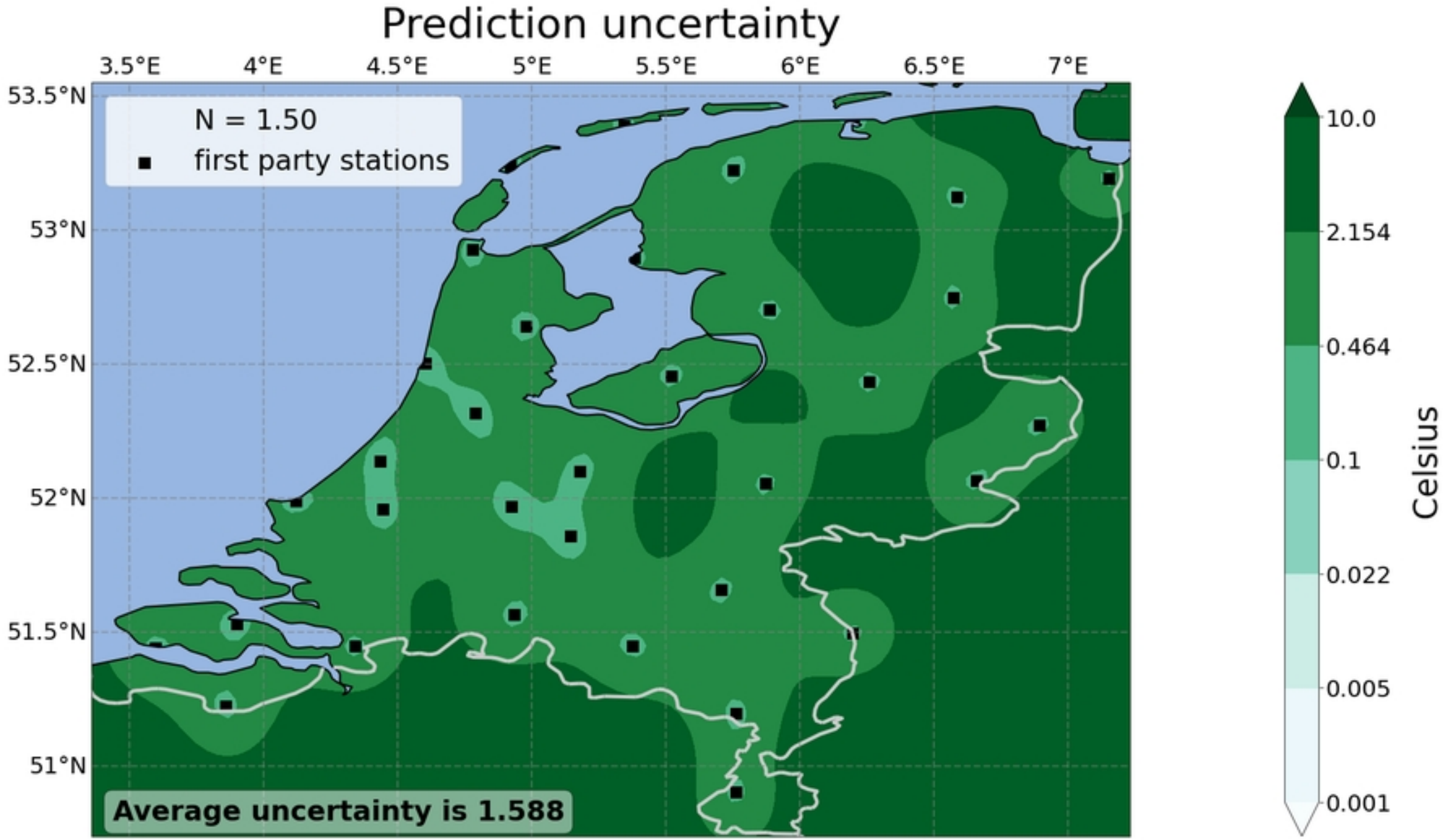
Prediction uncertainty
3.5°E
4°E
4.5°E
5°E
5.5°E
6°E
6.5°E
7°E
53.5°N
53°N
52.5°N
52°N
51.5°N
51°N
N = 1.50
first party stations
Average uncertainty is 1.588
10.0
2.154
0.464
0.1
0.022
0.005
0.001
Celsius

Figure7

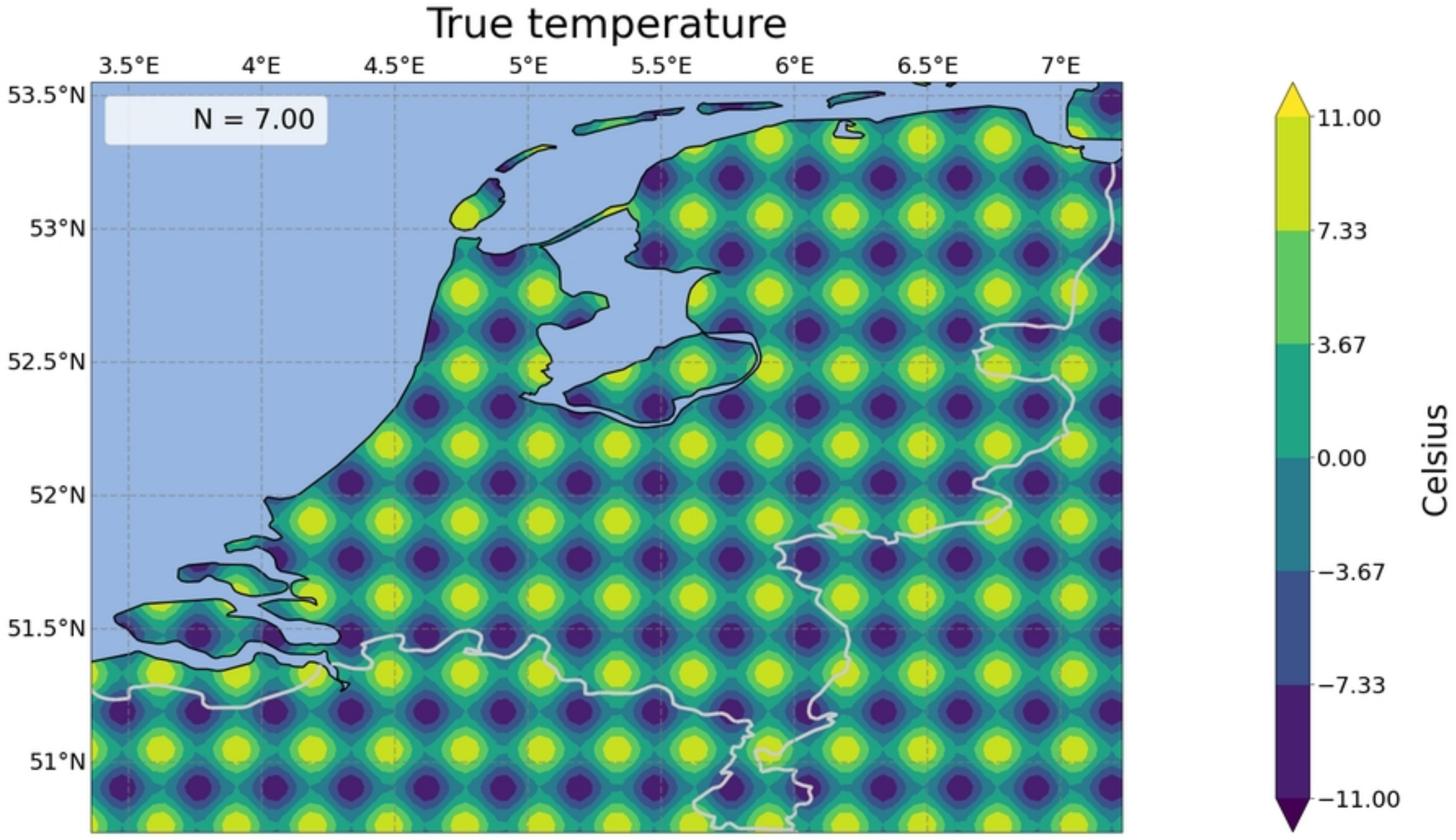
True temperature
3.5°E
4°E
4.5°E
5°E
5.5°E
6°E
6.5°E
7°E
53.5°N
53°N
52.5°N
52°N
51.5°N
51°N
N = 7.00
11.00
7.33
3.67
0.00
−3.67
−7.33
−11.00
Celsius

Figure8

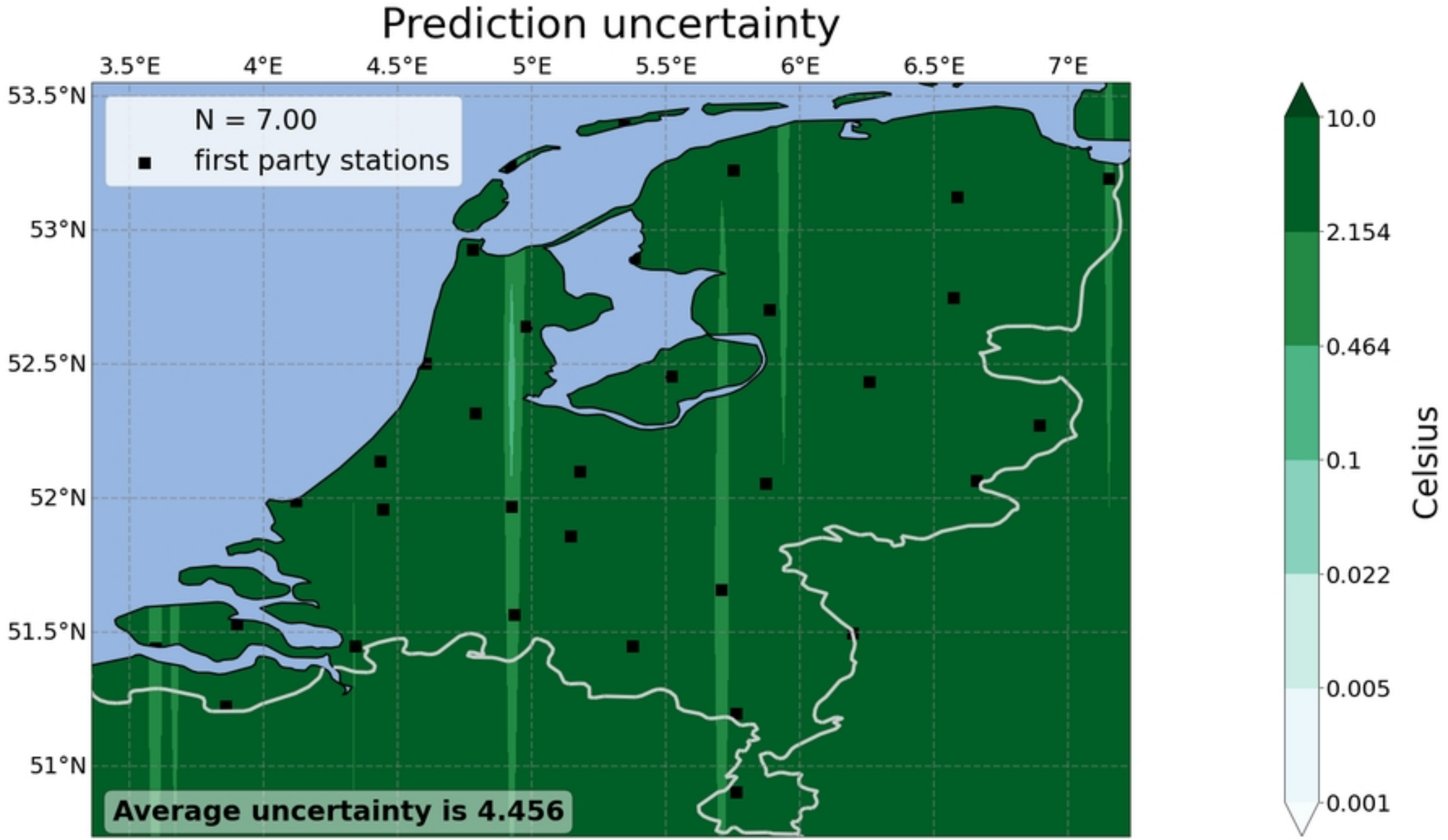
Prediction uncertainty
3.5°E
4°E
4.5°E
5°E
5.5°E
6°E
6.5°E
7°E
53.5°N
53°N
52.5°N
52°N
51.5°N
51°N
N = 7.00
first party stations
Average uncertainty is 4.456
10.0
2.154
0.464
0.1
0.022
0.005
0.001
Celsius

Figure9

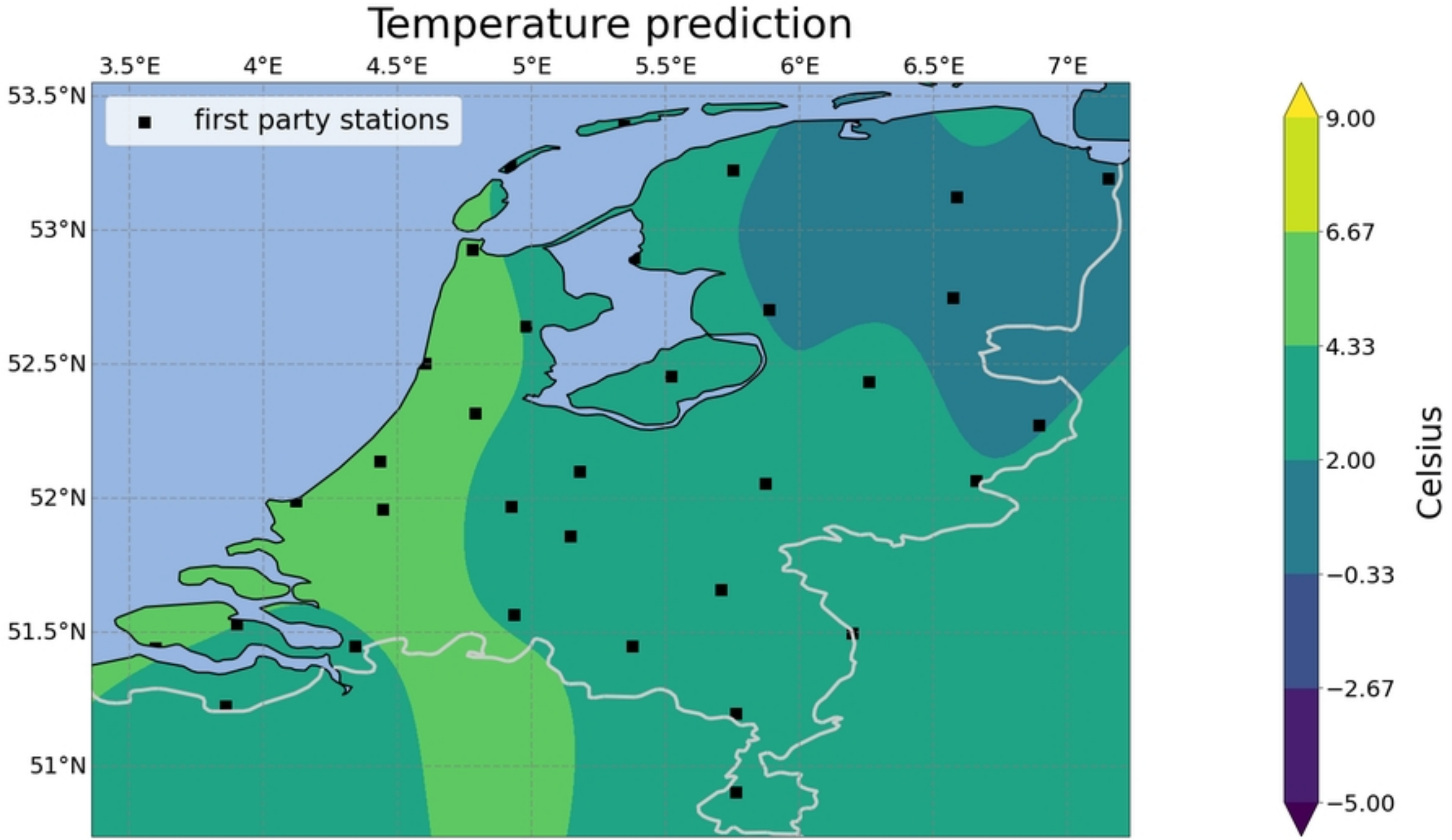
Temperature prediction
3.5°E
4°E
4.5°E
5°E
5.5°E
6°E
6.5°E
7°E
53.5°N
53°N
52.5°N
52°N
51.5°N
51°N
first party stations
9.00
6.67
4.33
2.00
−0.33
−2.67
−5.00
Celsius

Figure10

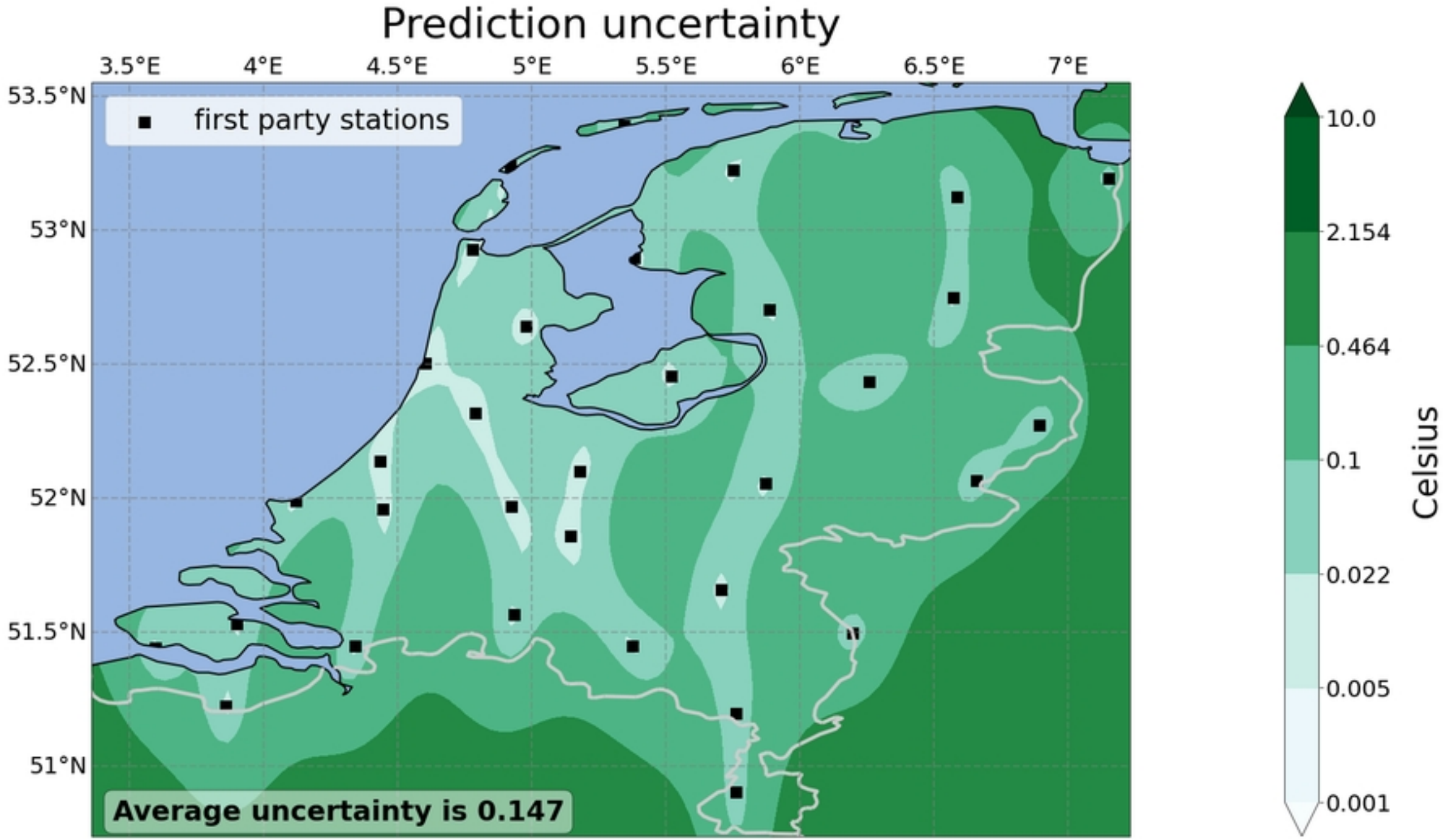
Prediction uncertainty
3.5°E
4°E
4.5°E
5°E
5.5°E
6°E
6.5°E
7°E
53.5°N
53°N
52.5°N
52°N
51.5°N
51°N
first party stations
Average uncertainty is 0.147
10.0
2.154
0.464
0.1
0.022
0.005
0.001
Celsius

Figure11

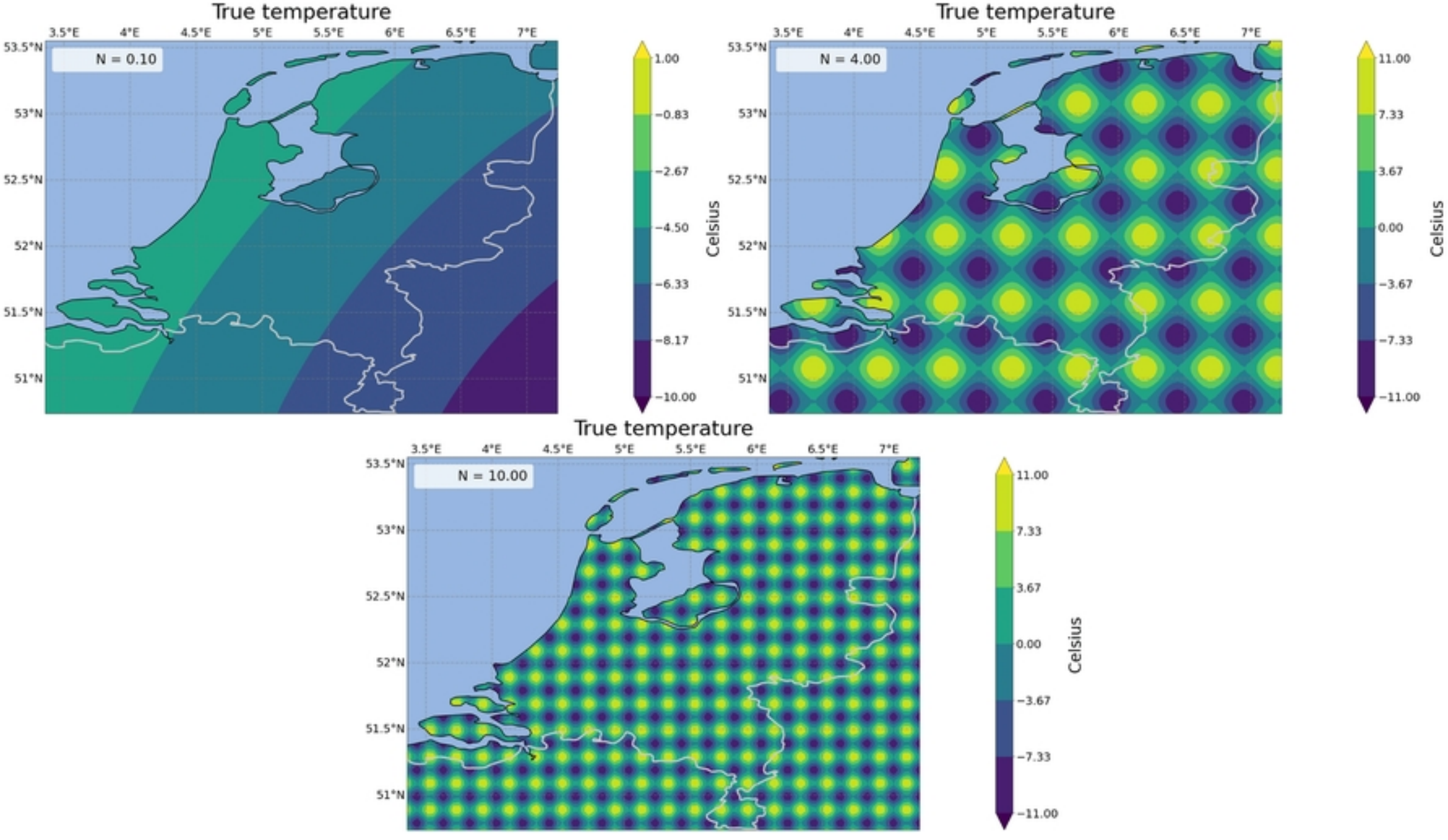
True temperature
N = 0.10
True temperature
N = 4.00
True temperature
N = 10.00
3.5°E
4°E
4.5°E
5°E
5.5°E
6°E
6.5°E
7°E
53.5°N
53°N
52.5°N
52°N
51.5°N
51°N
1.00
−0.83
−2.67
−4.50
−6.33
−8.17
−10.00
11.00
7.33
3.67
0.00
−3.67
−7.33
−11.00
Celsius

Figure2